Dalton Transactions

ROYAL SOCIETY OF CHEMISTRY

PAPER

View Article Online
View Journal | View Issue

Check for updates

Cite this: *Dalton Trans.*, 2021, **50**, 7400

Sensitised lanthanide luminescence using a Ru^{II} polypyridyl functionalised dipicolinic acid chelate†

Divya Rajah, Michael C. Pfrunder, Bowie S. K. Chong, Alexander R. Ireland, Isaac M. Etchells and Evan G. Moore *

Received 25th March 2021,
Accepted 26th April 2021

DOI: 10.1039/d1dt00982f

rsc.li/dalton

A visible light absorbing [Ru^{II}(tpy)$_2$]$^{2+}$-type chromophore appended with a dipicolinic acid Ln^{III} chelator has been prepared and complexed with several differing lanthanide cations to form the corresponding heterobimetallic d–f assemblies. The subseqent solution speciation analysed by ^{1}H NMR spectroscopy revealed an unexpected decrease in the Ln^{III} chelate complex stability, in particular for the 1 : 3 complex, when compared to the parent dipicolinic acid. As a result, the desired Ln(ML)$_3$ complexes could not be isolated, and the 1 : 1 Ln^{III}–ML complexes were instead characterised and investigated using steady state absorption and emission spectroscopy. Sensitised NIR emission from the Yb^{III}, Nd^{III} and Er^{III} complexes was observed upon ^{1}MLCT excitation of the Ru^{II} based metalloligand in the visible region at *ca.* 485 nm. Investigations using transient absorption spectroscopy revealed essentially quantitative intersystem crossing to form the ^{3}MLCT excited state, as expected, which then acts as the energy donor for the metalloligand based antennae effect, facilitating sensitisation efficiencies of 4.8, 17.0 and 37.4% respectively for the Yb^{III}, Er^{III} and Nd^{III} cations.

Introduction

The development of chelating d–f metalloligands which can function as light absorbing antennae for sensitised lanthanide emission, especially for near *infra*-red (NIR) emitting cations such as Yb^{III}, Er^{III} and Nd^{III}, has received considerable literature interest due to their highly desirable luminescence properties. For example, rapid Intersystem Crossing (ISC) and the typically long-lived triplet excited states of Ru^{II}, Os^{II} and Ir^{III} complexes makes them well suited for this purpose.[1,2] Indeed, a range of d–f complexes using these metals and a variety of polypyridyl type ligands such as 2,2′-bipyridine (bpy) or functionalised derivatives have been shown to exhibit efficient energy transfer and sensitisation of Ln^{III} luminescence.[3–6]

Considering Ru^{II} complexes more specifically, Klink *et al.* reported[7] several years ago that functionalised lanthanide complexes utilising *m*-terphenyl based Ln^{III} chelators appended with a [Ru^{II}(bpy)$_3$]$^{2+}$ chromophore could be used as an antenna to sensitise NIR Ln^{III} luminescence. Sénéchal-David *et al.* also demonstrated[8] that a macrocyclic Ln^{III} chelator functionalised with a [Ru^{II}(bpy)$_2$(phen)]$^{2+}$ complex can be an effective sensitiser for NIR emission, particularly with Nd^{III}. Not surprisingly, the observed Ln^{III} emission is longer-lived in D$_2$O compared to H$_2$O, due to the elimination of solvent oscillators which can otherwise lead to non-radiative quenching of the Ln^{III} emission.[9] In each of these cases, the distance between the transition metal and 4f metal ion was relatively short, and non-conjugated alkyl groups were used to link the components. Alternately, by utilising an extended aromatic π linked systems, Ward was able to demonstrate efficient sensitisation of NIR emitting Ln^{III} cations at distances of over *ca.* 20 Å *via* a Dexter type superexchange mechanism using a functionalised [Ru^{II}(bpy)$_3$]$^{2+}$ chromophore as the sensitiser.[10]

More recently, we reported the use of a functionalised [Ru^{II}(tpy)$_2$]$^{2+}$-type complex (tpy = 2,2′:6′,2″-terpyridine) as a sensitiser for Ln^{III} emission in the NIR region.[11] Despite the much shorter ^{3}MLCT lifetime of a bis-tridentate [Ru^{II}(tpy)$_2$]$^{2+}$ complex as an antenna chromophore, which can be attributed[12] to the structural distortion away from O_h symmetry, and the corresponding increase in non-radiative deactivation *via* low lying ^{3}MC excited states, we nonetheless demonstrated that relatively efficient sensitisation of NIR emitting 4f metals can be achieved using this type of antenna.

In this previous work[11] one of the tpy ligands bound to Ru^{II} was subsitituted in the 4′-position with an additional pendant tpy chelator, in order to facilitate formation of the desired d–f complex. However, it is quite well known that Ln^{III} complexes with purely N donor ligands generally suffer from lower

---

School of Chemistry and Molecular Biosciences, The University of Queensland, St Lucia, QLD, 4072, Australia. E-mail: egmoore@uq.edu.au

† Electronic supplementary information (ESI) available: Experimental and synthetic details, X-ray crystallographic data, additional NMR data, details for TD-DFT calculations and additional photophysical data. CCDC 2065117. For ESI and crystallographic data in CIF or other electronic format see DOI: 10.1039/d1dt00982f

aqueous stability constants (*e.g.* $[\mathrm{Lu^{III}(tpy)}]^{3+}$, $\log_{10}\beta_{110} = 2.8$), since the Lewis acidity of the ligand and metal ions are not well matched.[13] As an alternative, carboxylate groups which provide significantly harder and negatively charged O donor atoms, can lead to much higher stability constants. As a pertinent example, it has been established that pyridine-2,6-dicarboxylic acid, also known as dipicolinic acid (H_2DPA), is an efficient Ln^{III} chelator, and shows significantly larger formation constants (*e.g.* $[\mathrm{Lu^{III}(DPA)}_n]^{(3-2n)+}$, $\log_{10}\beta_{1n0} = 9.0$, 16.8 and 21.5 for $n = 1, 2, 3$), allowing for efficient formation of the tris $Ln^{III}(DPA)_3$ complexes in aqueous solution.[14] Upon excitation in the UV region *via* the π–π* transitions of the coordinated DPA^{2-} anion, several $[\mathrm{Ln^{III}(DPA)_3}]^{3-}$ complexes are known[15] to exhibit high sensitisation efficiencies ($\eta_{\mathrm{sens}} > 70\%$) and relatively good photo-luminescence quantum yields (PLQY), in particular with Tb^{III} and Eu^{III} of $\Phi = 21\%$ and 29% respectively. This can be attributed to preventing vibrational quenching by inner sphere solvent molecules such as water,[9] and these complexes have also been proposed[16] as suitable secondary standards for PLQY measurements of Ln^{III} complexes containing these cations. Notably, the $[\mathrm{Yb^{III}(DPA)_3}]^{3-}$ complex also displays sensitised emission in the NIR region at *ca.* 980 nm, although the evaluated PLQY is much smaller at only 0.015%, which has been attributed[15] to its lower sensitisation efficiency of *ca.* 8% due to the large energy gap between ligand donor states and the 4f* metal centered $^2F_{5/2}$ accepting state of Yb^{III}.

A variety of synthetic approaches have been reported for the development of functionalised H_2DPA derivatives as Ln^{III} sensitisers. For example, exploiting the 4-hydroxy substituted version (also known as chelidamic acid), covalent attachment of additional light absorbing organic sensitisers has been achieved by several groups.[14,17,18] For example, this approach was used to append a variety of different isomeric coumarin based chromophores *via* flexible polyether chains of variable length.[19] Interestingly, shortening the chain length resulted in practically no change in the overall quantum yields for the Eu^{III} complexes in solution, which was attributed to the inherent flexibility of the oligoethylene glycol linkage. Alternately, using a variety of Pd catalysed aryl/ethynyl cross coupling reactions, D'Aléo *et al.* have synthetically modified the H_2DPA chelate, again in the 4-position, allowing for a large family of push–pull π-conjugated ligands to be prepared in an effort to increase the two photon absorption (TPA) cross sections for the corresponding Eu^{III} complexes.[20] In this family of compounds, sensitised emission at 613 nm with PLQY's as high as 43% were demonstrated using low energy excitation wavelengths between 700–900 nm.

However, to the best of our knowledge, only one example of a modified H_2DPA chromophore bearing a pendant transition metal based chromophore has appeared in the literature. Quite recently, Xiong *et al.* reported[21] the synthesis of two novel H_2DPA based chelators, substituted with both free base or Pd(II) metalated chlorins *via* the 3- or 15-position of the latter. This series of antennae yielded the corresponding tris complexes with both Yb^{III} and Nd^{III}, and it was shown that excitation *via* the range of Q-band absorption maxima at *ca.* 600 nm yielded sensitized NIR emission in aqueous solution, with potential applications in multiplex fluorescence imaging.

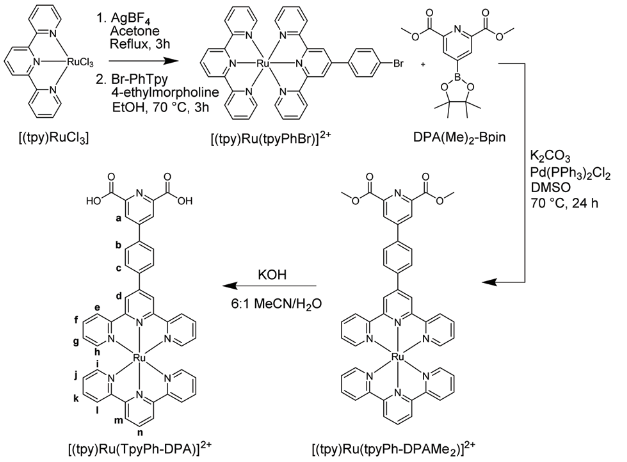

Scheme 1 Design and synthesis of the $[\mathrm{(tpy)Ru^{II}(tpyPh\text{-}DPA)}]^{2+}$ metalloligand.

Considering the limitations in terms of the solution stability for our previously reported[11] $[\mathrm{Ru^{II}(tpy)_2}]^{2+}$-type antenna based system, which featured a pendant 2,2′:6′,2″-terpyridine group to facilitate Ln^{III} chelation for d–f complex formation, we have redesigned this system as shown in Scheme 1, in order to incorporate a more Ln^{III} specific dipicolinic acid based chelator. However, we have retained the bis tridentate $[\mathrm{Ru(tpy)_2}]^{2+}$-type antenna, since this chromophore features a strong ^{1}MLCT absorption band in the visible region suitable for sensitisation of NIR emitting Ln^{III} cations. Similarly, ISC to form the ^{3}MLCT excited state energy donor can be considered to be essentially quantitative in these complexes,[22] and although their excited state lifetimes are significantly shorter than corresponding tris bidentate Ru^{II} polypyridyl complexes such as $[\mathrm{Ru(bpy)_3}]^{2+}$, we have shown[11] that if the rate of energy transfer for sensitised Ln^{III} emission *via* the antennae effect is sufficiently rapid, sizeable sensitisation efficiencies can still be achieved. Lastly, by utilising a 4-substituted H_2DPA chelate, it was envisaged that formation of the corresponding $[\mathrm{Ln(ML)_3}]^{3+}$ complexes in solution would result in improved luminescence performance, by both excluding inner sphere solvent molecules and increasing the number of energy donors *via* the formation of tris chelated d–f metallostars.[23]

Results and discussion

Synthesis and characterisation

The desired Ru^{II} metalloligand was prepared adopting a variety of literature methods[24–27] in the stepwise approach detailed in Scheme 1, which involved first constructing the appropriately mono substituted Ru^{II} based aryl halide, followed by an aryl cross coupling 'on-the-complex' and subsequent deprotection. To summarise, starting from chelidamic acid, which was esterified, brominated and then subjected to Miyaura borylation, an overall yield of 46% for the required coupling precursor was obtained. Notably, borylation of the brominated chelidamic following a literature procedure[20] in DMSO was unsuccessful in our hands, although an alternative method reported by Rasheed *et al.*[28] using dioxane as the solvent gave the desired product. In parallel, [$RuCl_3 \cdot H_2O$] was complexed with tpy followed by tpyPh-Br in an overall yield of 51% after chromatography. The subsequent Pd-catalysed Suzuki cross coupling reaction to form [(tpy)Ru^{II}(tpyPh-DPAMe$_2$)]$^{2+}$ was successful, albeit in a relatively low yield of 10%, which we attribute to loss of the methyl protecting groups under the slightly basic reaction conditions required, which necessitated tedious purification by column chromatography. Nonetheless, the methyl protected metalloligand was able to be isolated in high purity as a KPF_6 adduct, and was fully characterised using ^{1}H NMR, HRMS, CHN elemental analysis and X-ray crystallography.

The ^{1}H NMR spectrum of [(tpy)Ru^{II}(tpyPh-DPAMe$_2$)]$^{2+}$ in CD_3CN (see Fig. S1, ESI†), was fully assigned using ^{1}H–^{1}H COSY and 1D-NOESY techniques (see Fig. S2–S5, ESI†). Protons H_a, H_d and H_m, as labelled in Scheme 1, were readily assigned by comparison to the precursor [(tpy)Ru^{II}(tpyPh-Br)]$^{2+}$ complex, with proton H_a at 8.71 ppm appearing as the obvious new signal indicating the successful cross coupling. Proton H_d located at 9.08 ppm was used to identify the adjacent H_e and H_c protons *via* 1D-NOESY and the assignment was further confirmed by the observed ^{1}H–^{1}H COSY correlations. The assignments of proton H_b and H_c signals was confirmed by irradiation of H_a as well as ^{1}H–^{1}H COSY correlations. Proton H_m was identified by the ^{1}H–^{1}H COSY correlation with H_n, and subsequently used to identify H_l by an observed 1D-NOESY signal, allowing the remaining pyridyl protons to be assigned using ^{1}H–^{1}H COSY correlations.

Slowly evaporating a solution of the methyl protected metalloligand in an acetonitrile water mixture allowed crystals suitable for X-ray studies to be obtained. Although these were of generally poor quality and were found to be a two-fold twin about the [−105] lattice direction, the structure was nonetheless able to be solved in the $P\bar{1}$ space group, and was formulated as the [(tpy)Ru^{II}(tpyPh-DPAMe$_2$)](PF$_6$)$_2$·KPF$_6$ adduct, allowing the connectivity of the complex to be unambiguously determined. A single Ru^{II} metalloligand as its bis hexafluorophosphate salt together with an additional KPF_6 moiety were located in the asymmetric unit, with the complex cations packed into 1D chains oriented along the *c* axis. A poorly ordered PF_6^- anion is positioned between the adjacent Ru^{II} cations, and shows two non-classical H-bonding interactions between two fluorine atoms and the protons of two neighbouring complexes (F17–H2 = 2.407 Å, F14–H12 = 2.252 Å). Notably, the DPAMe$_2$ binding site contains a single potassium cation, with an overall coordination number of 10, which is bound to the two O alkoxy atoms and the pyridyl N atom. The coordination sphere of the alkali metal is completed by a mixture of bidentate and monodentate K–F interactions with adjacent disordered PF_6^- ions, which form a ribbon along the *b* axis, completing the overall charge balance (Fig. 1).

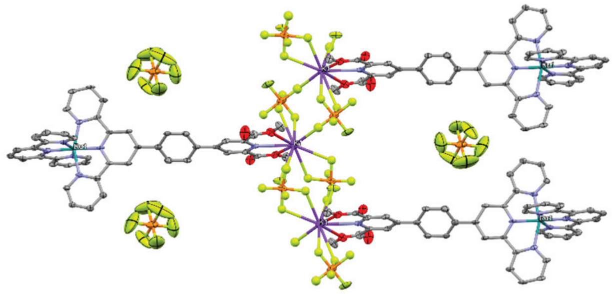

Fig. 1 View of the X-ray structure for the [(tpy)Ru^{II}(tpyPh-DPAMe$_2$)](PF$_6$)$_2$·KPF$_6$ complex, emphasising molecular packing. Thermal ellipsoids are shown at the 50% probability level and H atoms are omitted for clarity. C (grey), N (blue), O (red), P (orange), F (yellow), P (purple), and Ru (teal).

The Ru^{II} ion shows a distorted octahedral coordination sphere, with average Ru–N bond lengths of 2.043 and 2.033 Å for the capping and bridging tpy ligands respectively. As expected, the Ru–N bond lengths for the peripheral tpy pyridyl rings are slightly longer (avg. = 2.073 Å) than the central pyridyl bond lengths (avg. = 1.968 Å). The tpy ligands are approximately perpendicular with each other, with an interplanar angle of 88.5°. The phenyl linker between the chelated tpy and DPAMe$_2$ groups shows a torsion angle of 51.2° relative to tpy, or 32.6° relative to the DPAMe$_2$ moiety, resulting in the tpy and DPAMe$_2$ moieties being oriented approximately perpendicularly at 84.5°.

To complete the required synthesis, the methyl deprotected [(tpy)Ru^{II}(tpyPh-DPA)] metalloligand was obtained by hydrolysis of the corresponding dimethyl ester in the presence of excess KOH in an acetonitrile/water solvent mixture (6 : 1 v/v) followed by the addition of HPF_6 to precipitate the desired product in good yield and analytically pure form as determined by ^{1}H NMR, CHN and HRMS analysis. Notably, hexafluorophosphoric acid was used necessarily in this step rather than an anionic PF_6^- salt, to avoid formation of an otherwise zwitterionic complex, which we found was resistant to isolation by precipitation.

The ^{1}H NMR obtained for [(tpy)Ru^{II}(tpyPh-DPA)], shown in Fig. 2 (see also Fig. S6, ESI†), was fully assigned by comparison to the spectra for the [(tpy)Ru^{II}(tpyPh-DPAMe$_2$)]$^{2+}$ complex, since, although different solvents were used, the observed signals display essentially identical splitting patterns and quite similar chemical shifts, with the exception of a small upfield shift for the H_a signal (*ca.* 0.15 ppm), small downfield shifts for the H_d, H_m, H_e and H_l signals (*ca.* 0.1–0.2 ppm), and the obvious disappearance of the methyl ester signal at 4.03 ppm.

Speciation and solution stability

Formation of the desired d–f complexes was investigated using ^{1}H NMR spectroscopy to monitor the titration of Lu

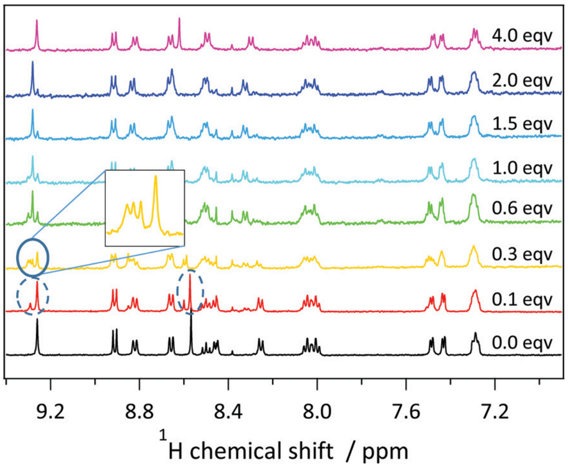

Fig. 2 ^{1}H NMR titration for a 0.2 mM solution of [(tpy)Ru^{II}(tpyPh-DPA)] in MES buffered 2 : 1 MeOD : D_2O (v/v) solution (0.1 M, pD ~ 6.4) upon addition of [Lu(OTf)$_3$·6H_2O].

(OTf)$_3$·6H_2O into a 0.2 mM solution of the [(tpy)Ru^{II}(tpyPh-DPA)] complex in a MES buffered solution (MES = 2-(*N*-morpholino)ethanesulfonic acid, 0.1 M, pD ≈ 6.4) of 2 : 1 MeOD : D_2O (v/v), with results as summarised in Fig. 2.

Upon addition of 0.1 molar equiv. of Lu(OTf)$_3$·6H_2O, the ^{1}H NMR spectrum shows only minor changes, although particularly noticeable is the appearance of two new singlet peaks at 9.29 and 8.60 ppm (also highlighted in Fig. 2 by dashed circles), which we attribute to the H_a and H_d protons of the Lu(ML)$_3$ complex, which should form preferentially in the presence of an excess of the ML metalloligand (where ML = [(tpy)Ru^{II}(tpyPh-DPA)].

$$3\ \mathrm{ML} + \mathrm{Ln} \rightleftharpoons \mathrm{Lu(ML)_3} \tag{1}$$

Subsequent addition of Lu^{III} shows further changes in the ^{1}H NMR signals. For example, the spectrum obtained after the addition of 0.3 molar equiv. clearly shows the appearance of four different singlet peaks at *ca.* 9.25 ppm, which we have assigned to the H_d protons of d–f complexes with ML, Ln(ML), Ln(ML)$_2$, and Ln(ML)$_3$ stoichiometry formed upon the addition of increasing equivalents of the Lu^{III} metal ion.

$$\mathrm{Ln(ML)_3} + \mathrm{Ln} \rightleftharpoons \mathrm{Ln(ML)_2} + \mathrm{Ln(ML)} \tag{2}$$

Further addition of Lu(OTf)3·6H_2O reveals a continued decrease in the amount of 3 : 1 and 2 : 1 d–f complexes. Similarly, this data also shows that at least two species are present in solution until an excess (4.0 molar equiv.) of Lu^{III} has been added, resulting in exclusive formation of the 1 : 1 d–f complex.

$$\mathrm{Ln(ML)_2} + \mathrm{Ln} \rightleftharpoons 2\ \mathrm{Ln(ML)} \tag{3}$$

At the end of the titration, formation of the 1 : 1 d–f complex was particularly evident for H_a and H_d, which shifted downfield during the titration from 8.57 to 8.62 and 9.26 to 9.28 ppm respectively. More importantly, the ^{1}H NMR data also revealed that the desired Ln(ML)$_3$ ‹metallostar' complexes could not be isolated with the [(tpy)Ru^{II}(tpyPh-DPA)] metalloligand, due to the equilibria involved in tris complex formation.

In order to assess the individual complex formation constants, the corrected integrals for each of the species attributed to the ML, Ln(ML), Ln(ML)$_2$ and Ln(ML)$_3$ complexes have been fitted to four overlapping Lorentzian functions (see Fig. S7, ESI†), and hence the concentration of each species was evaluated. A best fit of the observed *versus* calculated percentage speciation data using HySS2009[29] allowed the cumulative stability constants to be estimated as $\log_{10}\beta_{110}$ = 4.8(1), $\log_{10}\beta_{120}$ = 8.3(1), and $\log_{10}\beta_{130}$ = 11.4(1) (see Fig. S8, ESI†). Notably, these values are several orders of magnitude smaller than those of the DPA^{2-} anion,[14] which we attribute to the electron withdrawing Ru^{II} complex that is covalently appended to the pyridine-2,6-dicarboxylate, significantly decreasing its chelating ability.

Since the solution thermodynamic model demonstrated formation of the 3 : 1 d–f complexes would not be possible at concentrations suitable for photophysical measurements, the properties of the 1 : 1 d–f complexes were instead investigated. As an additional verification that the [(tpy)Ru^{II}(tpyPh-DPA)] complex binds other Ln^{III} cations as the 1 : 1 Ln(ML) complex, addition of an excess of Nd^{III}(OTf)$_3$·6H_2O to a solution of the metalloligand was also undertaken, and was analysed by ^{1}H NMR spectroscopy, resulting in much larger downfield chemical shifts for various protons, including H_a, due to the presence of the paramagnetic metal ion (see Fig. S9, ESI†).

Density functional theory

In order to improve our understanding on the nature of the excited states for both the [(tpy)Ru^{II}(tpyPh-DPA)] metalloligand and the corresponding 1 : 1 heterobimetallic d–f [(tpy)Ru^{II}(tpyPh-DPA)Ln^{III}(H_2O)$_x$]$^{3+}$ complexes, we have undertaken both static and time dependent (TD) density functional theory (DFT) calculations, using an mPW1PW91 functional and mixed D95 V/LanL2TZ(f)/def2-QZVP basis sets using an SMD solvation model with methanol (for further details, see the ESI†).

The resulting optimised geometries and selected frontier molecular orbitals for the [(tpy)Ru^{II}(tpyPh-DPA)] complex and corresponding [(tpy)Ru^{II}(tpyPh-DPA)Lu^{III}(H_2O)$_5$]$^{3+}$ d–f complex are shown in Fig. 3. Notably, the calculated structure of [(tpy)Ru^{II}(tpyPh-DPA)] is very similar to the structure of the dimethylester derivative obtained by X-ray crystallography. The coordination geometry about the Ru^{II} centre is a distorted octahedron, with capping and bridging tpy moieties in a planar orientation and average Ru–N bond lengths of *ca.* 2.03 Å, which are almost identical to those found in the X-ray structure of 2.04 Å. As expected, slightly shorter Ru–N bond lengths to the central tpy N atom are evident, due to the strained chelate ring, which also leads to N–Ru–N bond angles for each of the chelated tpy moieties which deviate from the ideal 90° to approximately 79°. The non-coordinated DPA^{2-} moiety is also twisted at an angle of *ca.* 66° with respect to the chelated tpy moiety.

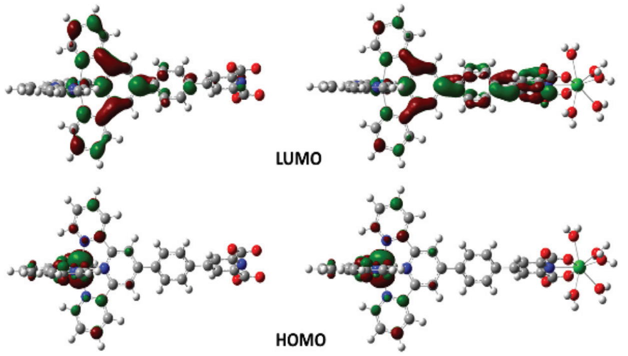

Fig. 3 Optimised DFT geometries of [(tpy)Ru^{II}(tpyPh-DPA)] (left) and [(tpy)Ru^{II}(tpyPh-DPA)Lu^{III}(H$_2$O)$_5$]$^{3+}$ (right) and selected HOMO and LUMO molecular orbitals.

For the heterobimetallic d–f complex, the diamagnetic Lu^{III} cation was chosen as a general model for the bound Ln^{III} cations presented in this study. The calculated geometry around the Lu^{III} cation is as expected, showing tris coordination to the deprotonated DPA^{2-} moiety of the bridging ligand, with an average Lu^{III}–O bond length of 2.29 Å, and Lu^{III}–N bond length of 2.39 Å. The distance between the Ru^{II} donor and Ln^{III} acceptor was estimated to be approximately 15.8 Å (see Fig. S10, ESI†). Notably, we have modelled the remainder of the coordination sphere for the Lu^{III} metal ion with five coordinated solvent water molecules, in accordance with a known literature precedent.[30] While this is most likely to be the case for the smaller Ln^{III} cations (*e.g.* Er^{III}, Yb^{III} and Lu^{III}) due to their smaller ionic radius, it is possible that the larger Ln^{III} cations (*e.g.* Nd^{III}) may exist with either five or six coordinated solvent water molecules bound to the metal ion. While this difference in solvation will certainly influence many of the luminescent properties, such as the 4f* centered PLQY, it is not of particular relevance in terms of the ligand centered sensitisation efficiencies presented herein (*vide infra*).

An analysis of the relevant molecular orbitals obtained from TD-DFT studies reveals that the HOMO and LUMO for both the metalloligand and corresponding d–f complex have significant orbital densities located on the Ru^{II} metal center and bridging tpyPh-DPA ligand respectively (see Fig. 3, Table S1, and Fig. S11 and S12, ESI†). For the [(tpy)Ru^{II}(tpyPh-DPA)] metalloligand, the predominant contributions for the lowest energy singlet (S$_1$) excited state are from the HOMO → LUMO (96.4%) orbitals, while the lowest energy triplet (T$_1$) excited state involves predominantly the HOMO−1 and LUMO (83.7%) orbitals. As noted, the majority of the electron density is localised on the Ru^{II} center for the HOMO/HOMO−1, while the LUMO is located primarily on π* type orbitals on the tpy group of the bridging tpyPh-DPA ligand, consistent with the lowest energy singlet and triplet excited states having MLCT excited state character. A comparison of the calculated UV-Vis absorption spectrum to the experimental spectrum (see Fig. S13, ESI†) shows very good agreement. The corresponding 1 : 1 d–f complex with Lu^{III} also displays electronic transitions which predominantly involve the HOMO → LUMO (81.4%) and HOMO−1 → LUMO (73.5%) for the lowest energy S$_1$ and T$_1$ excited state respectively, with the simulated spectrum again showing an excellent match to the experimental spectrum (see Fig. S14, ESI†).

It is interesting to note that when the Lu^{III} cation is chelated to the DPA moiety, the corresponding LUMO involved in the lowest energy singlet and triplet excited states appears to be more localised over the pyridine-2,6-dicarboxylate end of the tpyPh-DPA ligand, an effect which was less pronounced for the free metalloligand. It is enticing to contemplate whether the observed localisation in close proximity to the 4f metal ion may enhance the rate of EET involved in sensitised Ln^{III} emission.

Photophysical properties

The steady state UV-Vis absorption and emission spectra of the [(tpy)Ru^{II}(tpyPh-DPA)] metalloligand is shown in Fig. 4, using a MES buffered (0.1 M, pD 6.4) 2 : 1 MeOD : D$_2$O (v/v) solvent system. As expected, the absorption spectrum features several peaks in the UV region at *ca.* 220, 270 and 310 nm, which correspond to π → π* transitions of the aromatic DPA^{2-} and tpy groups, in agreement with previous literature examples.[11,31,32] In the visible region, a strong characteristic peak at *ca.* 485 nm is also observed which we attribute to the Ru^{II} ^{1}MLCT absorption band, and is again similar to those reported for [Ru(tpy)$_2$]$^{2+}$-type derivatives.[11,32] Excitation of the metalloligand at *ca.* 485 nm leads to a broad emission band centred at *ca.* 662 nm, which can be attributed to ^{3}MLCT phosphorescence. Although quite weak, ^{3}MLCT emission has been observed in similar [Ru(tpy)$_2$]$^{2+}$ complexes bearing extended aryl ligands.[33,34]

In order to investigate their photophysical properties, the corresponding 1 : 1 d–f complexes with Ln^{III} = Lu, Yb, Er and Nd were formed *in situ* by adding an excess (>5 molar equiv.) of the corresponding Ln(OTf)$_3$ salt to a stock solution of the free metalloligand, again using the same concentration and

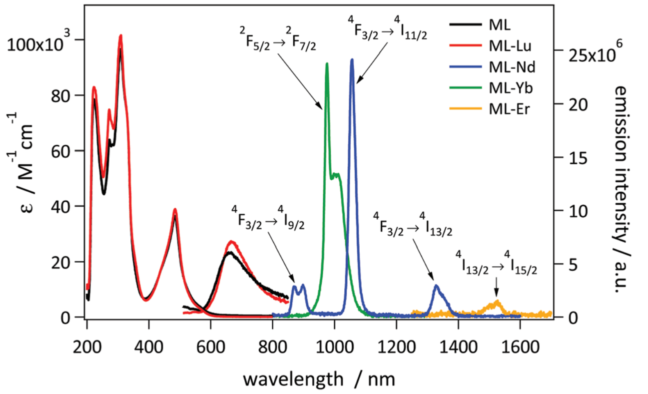

Fig. 4 UV-Vis absorption (left) and emission spectra (λ_{ex} = 485 nm, right) for 0.2 mM solutions of 1 : 1 ML–Ln complexes where ML = [(tpy)Ru^{II}(tpyPh-DPA)] and Ln = Lu, Nd, Yb or Er in MES buffered (0.1 M, pD ~ 6.4) 2 : 1 d$_4$-MeOD : D$_2$O (v/v).

mixed solvent system as that used for the ^{1}H NMR solution speciation studies.

The UV-Vis spectra for the [(tpy)Ru^{II}(tpyPh-DPA)Lu^{III}(H$_2$O)$_5$]$^{3+}$ complex is shown in Fig. 4 (see also Ln^{III} = Nd, Yb, Er complexes in Fig. S15, ESI†). Notably, coordination of Ln^{III} cations to the DPA^{2-} chelate is accompanied by only a small increase in the absorbance of the d–f complexes in the UV region at *ca.* 270 nm, while the ^{1}MLCT peak in the visible region appears relatively unchanged upon 1 : 1 d–f complex formation. This is consistent with previous reports[35,36] using related DPA^{2-} derivatives, which show only small changes upon spectrophotometric titration with Ln^{III} cations. In the present case, the change in the UV region is also relatively small due to the differences expected in the molar extinction coefficients of the DPA^{2-} (*ca.* 5000 M^{-1} cm^{-1}) compared to the [Ru(tpy)$_2$]$^{2+}$ fragments (>30 000 M^{-1} cm^{-1}).[26,37] By contrast, the emission spectra for the 1 : 1 d–f complexes using excitation *via* the ^{1}MLCT absorption peak (λ_{ex} = 485 nm) showed more significant differences. For [(tpy)Ru^{II}(tpyPh-DPA)Lu^{III}(H$_2$O)$_5$]$^{3+}$, the observed ^{3}MLCT visible emission band centered at *ca.* 667 nm was red-shifted by 5 nm compared to the free metalloligand as shown in Fig. 4, and is noticeably sharper, with a FWHM of *ca.* 2370 cm^{-1} compared to *ca.* 2800 cm^{-1} for the latter (see also Fig. S16, ESI†). Moreover, excitation of the Near Infra-Red (NIR) emitting d–f complexes with Ln^{III} = Nd, Yb and Er display variable quenching of the ^{3}MLCT visible emission (Fig. S16, ESI†) compared to an isoabsorbing solution of the Lu^{III} complex, and instead exhibit NIR emission bands which are characteristic for each 4f metal ion. For the [(tpy)Ru^{II}(tpyPh-DPA)Yb^{III}(H$_2$O)$_5$]$^{3+}$ complex, an emission band at *ca.* 980 nm is evident, which corresponds to the ^{2}F$_{5/2}$ → ^{2}F$_{7/2}$ transition of the Yb^{III} cation. For the 1 : 1 d–f complex with Nd^{III}, three sharp emission bands at *ca.* 890 nm, 1055 nm, and 1325 nm are observed for the Nd^{III} centered ^{4}F$_{3/2}$ → ^{4}I$_J$ transitions (J = 9/2, 11/2, 13/2). Lastly, albeit weak, the ^{4}I$_{13/2}$ → ^{4}I$_{15/2}$ transition of the Er^{III} cation can also be observed at *ca.* 1520 nm for the corresponding Er^{III} complex. Accordingly, we can confirm that selective excitation of the ^{1}MLCT absorption band in the [Ru(tpy)$_2$]$^{2+}$-type chromophore, followed by rapid ISC to form the ^{3}MLCT excited state leads to sensitised NIR emission for these cations, as expected, *via* the antennae effect.

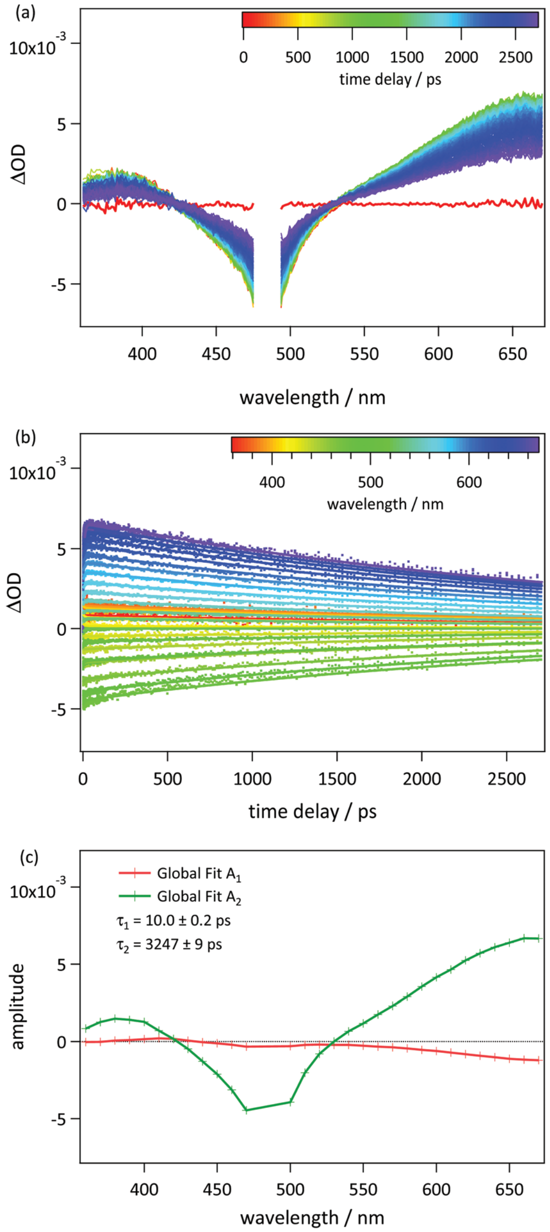

Fig. 5 (a) fs-TA spectra (λ_{ex} = 485 ± 10 nm removed), (b) globally fitted decay kinetics, (c) and decay associated difference spectra (DADS) including fitted lifetimes for the [(tpy)Ru^{II}(tpyPh-DPA)Yb(H$_2$O)$_5$]$^{3+}$ complex in MES buffered (0.1 M, pD ~ 6.4) 2 : 1 d$_4$-MeOD : D$_2$O (v/v).

Energy transfer kinetics

To gain a more detailed insight into the excited state dynamics of the observed antennae effect which leads to sensitised Ln^{III} emission, we have utilised femtosecond time resolved Transient Absorption (TA) spectroscopy, with the resulting spectra and decay kinetics for the 1 : 1 d–f complex with Yb^{III} shown as an example in Fig. 5 (see also Fig S17–S20 ESI† for other complexes). Upon ^{1}MLCT excitation at 485 nm, the TA spectra show three distinct transient features, including two positive excited state absorption (ESA) signals centered at *ca.* 380 nm and 650 nm, together with a strong negative signal centered at *ca.* 485 nm corresponding to ground state bleach (GSB) of the ^{1}MLCT absorption band. Importantly, the TA features observed for [(tpy)Ru^{II}(tpyPh-DPA)] and the corresponding [(tpy)Ru^{II}(tpyPh-DPA)Ln^{III}(H$_2$O)$_x$]$^{3+}$ complexes with Ln = Lu^{III}, Yb^{III}, Er^{III}, Nd^{III} were all essentially identical, and differed only in terms of the observed decay kinetics which were obtained by global fitting using the equation;

$$I_{(t)} = A_1 \exp^{-k_1 t} + A_2 \exp^{-k_2 t} \qquad (4)$$

where $I_{(t)}$ is the intensity of the observed TA signal, k_1 and k_2 are the fitted decay rates ($\tau_1 = 1/k_1$, *etc.*), while A_1 and A_2 are pre-exponential scaling factors. In the present case, based on

Table 1 Summary of observed decay lifetimes and resulting kinetic parameters obtained by fs-TA spectroscopy (λ_{ex} = 485 nm) for ML = [(tpy)Ru^{II}(tpyPh-DPA)] and the corresponding 1 : 1 ML–Ln^{III} complexes with Ln = Lu, Yb, Er and Nd in MES buffered (0.1 M, pD ~ 6.4) 2 : 1 d$_4$-MeOD : D$_2$O (v/v)

	τ_1 (vib) (ps)	τ_2 (^{3}MLCT) (ps)	$k_{obs}{}^a$ ($\times 10^8$ s^{-1})	k_{EET} ($\times 10^7$ s^{-1})	$\Phi_{EET}{}^{b,c}$ (%)
ML	9.6 ± 0.1	2301 ± 4	4.346 ± 0.008	N/A	N/A
ML-Lu	12.1 ± 0.2	3412 ± 9	2.931 ± 0.008	N/A	N/A
ML-Yb	10.0 ± 0.2	3247 ± 9	3.079 ± 0.009	1.5 ± 0.1	4.8 ± 0.4
ML-Er	10.1 ± 0.2	2831 ± 6	3.532 ± 0.008	6.0 ± 0.1	17.0 ± 0.3
ML-Nd	11.5 ± 0.2	2136 ± 4	4.681 ± 0.009	17.5 ± 0.1	37.4 ± 0.3

[a] k_{obs} (^{3}MLCT) = $1/\tau_2$. [b] $\Phi_{EET} = k_{EET}/k_{obs}$. [c] $\Phi_{EET} = \eta_{sens}$ (since $\Phi_{ISC} \approx 100\%$).

the relatively featureless decay associated difference spectrum (DADS) shown in Fig. 5(c), and several literature precedents,[38] we attribute the short-lived lifetime (τ_1) to vibrational cooling and solvent reorganisation of the ^{3}MLCT excited state formed by ISC from the initially populated ^{1}MLCT state upon photoexcitation. Instead, the longer lived lifetime (τ_2) is attributed to decay of the relaxed ^{3}MLCT excited state.

A summary of the excited state lifetimes obtained for the free metalloligand and each of the 1 : 1 d–f complexes is given in Table 1. For [(tpy)Ru^{II}(tpyPh-DPA)], the ^{3}MLCT lifetime obtained is *ca.* 2.3 ns, which is consistent with the known short lifetimes of [Ru(tpy)$_2$]$^{2+}$-type complexes (*e.g.* compared to [Ru(bpy)$_3$]$^{2+}$ derivatives), due to rapid non-radiative deactivation *via* the Ru^{II} metal centered (^{3}MC) excited state.[32] Upon complexation with Lu^{III}, the ^{3}MLCT lifetime of the resulting [(tpy)Ru^{II}(tpyPh-DPA)Lu^{III}(H$_2$O)$_5$]$^{3+}$ complex is slightly longer-lived, which can be rationalised by an increase in the rigidity of the ensuing d–f complex, and is also consistent with the observed sharpening of the steady state ^{3}MLCT emission. For the other 1 : 1 d–f complexes with Ln^{III} = Yb, Er, or Nd, the observed ^{3}MLCT lifetime decreases compared to the Lu^{III} complex in a manner which reflects the observed quenching of the steady state visible emission spectra. Again, this can be readily attributed to energy transfer with the ^{3}MLCT excited state acting as the energy donor, leading to sensitised NIR emission for these cations.

Using the observed lifetimes, the rate of energy transfer from the ^{3}MLCT excited state donor to 4f* excited state acceptor can also be calculated. Specifically, due to the absence of low energy 4f* excited states available for the Lu^{III} cation, the ^{3}MLCT lifetime of this complex can be used as a suitable model for deactivation of the [Ru(tpy)$_2$]$^{2+}$-type chromophore in the absence of competing energy transfer to NIR emitting cations. The sum of the radiative and non-radiative deactivation rate constants ($k_{obs} = k_r + k_{nr}$) is obtained from the observed lifetime using eqn (5) in the presence and absence of the NIR emitting Ln^{III} quencher. By making the reasonable assumption that k_r and k_{nr} for the ^{3}MLCT excited state energy donor are the same (*i.e.* independent of the 4f metal ion), the rate of electronic energy transfer (k_{EET}) can then be calculated from the difference in observed k_{obs} using eqn (6) below.[10,32,39]

$$\tau = \frac{1}{k_{obs}} \tag{5}$$

$$k_{EET} = k_{obs}(\text{NIR emitting Ln}) - k_{obs}(\text{Lu}) \tag{6}$$

$$\Phi_{EET} = \frac{k_{EET}}{k_{obs}} \tag{7}$$

Using these calculated k_{EET} values, and since ISC can be assumed[22] to be essentially quantitative for the Ru^{II} complexes ($\Phi_{ISC} \approx 100\%$), the energy transfer efficiency (Φ_{EET}) and also the overall sensitisation efficiencies ($\eta_{sens} = \Phi_{ISC} \times \Phi_{EET}$) for each of the NIR emitting Ln^{III} complexes can be evaluated from the ratio of k_{EET} to k_{obs} as shown in eqn (7). The resulting rates and efficiencies for the observed ^{3}MLCT → 4f* energy transfer are shown in Table 1.

To summarise, for each of the 1 : 1 d–f complexes with NIR emitting Ln^{III} cations (Ln = Nd, Yb and Er), the presence of low energy 4f* excited states for these metals facilitates energy transfer from the ^{3}MLCT excited state donor, resulting in both quenching of the emission intensity, and a significant decrease in the luminescence lifetime of the ^{3}MLCT state compared to the Lu^{III} model complex. For the Nd^{III} and Er^{III} complexes, which have a variety of potentially accepting 4f* excited states and considerable spectral overlap with the Ru^{II} ^{3}MLCT emission, the energy transfer rates (k_{EET}) we obtain are considerably faster than those with Yb^{III}, which has only a single $^2F_{5/2}$ accepting state. Nonetheless, despite the relatively short lifetime of the [Ru(tpy)$_2$]$^{2+}$-type chromophore, the energy transfer (and overall sensitisation efficiencies) are as high as *ca.* 37% with Nd^{III}.

Importantly, these results also agree well with previous observations we reported[11] using a [(toltpy)Ru^{II}(tpyPh-tpy)]$^{2+}$ metalloligand as the antennae chromophore (where toltpy = 4′-(*p*-tolyl)-2,2′:6′,2″-terpyridine, and tpyPh-tpy = 1,4-di([2,2′:6′,2′-terpyridin]-4′-yl)benzene). Moreover, the k_{EET} rates we obtain herein are also consistent and very similar to those obtained with this previous system, as we would expect due to the similar intramolecular separation between metal ions. Accordingly, the observed energy transfer we observe for the 1 : 1 d–f complexes reported herein can similarly be attributed to a Dexter type superexchange mechanism, as was the case previously, and which is also consistent with earlier reports[10] by Ward *et al.* who studied the distance dependence for Ru^{II} (^{3}MLCT) → Ln^{III} energy transfer using a series of structurally analogous aryl substituted [Ru(bpy)$_3$]$^{2+}$-type derivatives.

Conclusions

A $[Ru^{II}(tpy)_2]^{2+}$-type metalloligand functionalised with a dipicolinic acid chelate has been synthesised and characterised as a visible light absorbing antennae for sensitised Ln^{III} emission, since complexes of this type may be useful for the further development of NIR emitting biological imaging agents. Unfortunately, the anticipated formation of 3 : 1 d–f complexes was not successful, due to a decrease in the complex stability constants, which were found to be orders of magnitude lower than the DPA^{2-} ligand. This unanticipated result, attributed to a decrease in chelate strength due to the adjacent Ru^{II} complex, thwarted our attempts to characterise the photophysical properties of the desired 3 : 1 metallostar complexes.

Characterisation of the 1 : 1 d–f complexes was undertaken instead, and sensitised NIR emission using Ln^{III} = Nd, Yb and Er was demonstrated. Moreover, using steady state emission and transient absorption techniques, we were able to establish the thermalised Ru^{II} ^{3}MLCT excited state acts as an energy donor, after initial ^{1}MLCT excitation and rapid ISC. Analysis of the decay kinetics allowed both the energy transfer rate and sensitisation efficiencies to be estimated, and these were found to be similar to a series of $[(toltpy)Ru^{II}(tpyPh\text{-}tpy)Ln^{III}(NO_3)_3]$ complexes (Ln = Nd, Yb) we reported previously.[11] Considering their structural similarity, and the almost identical separation between the Ru^{II} and *4*f metal ions, the mechanism for the observed energy transfer has been attributed to a Dexter type superexchange, which is also consistent with previous reports.[10]

Considering the results reported herein, it is obvious that decreasing the intramolecular separation between metals ions should lead to a faster rate of energy transfer and improved sensitisation efficiencies for Ln^{III} emission, and our efforts toward preparing $[Ru^{II}(tpy)_2]^{2+}$-type metalloligands with shorter linkers will be reported in due course. Similarly, fusing a $[Ru^{II}(tpy)_2]^{2+}$ antennae chromophore to a multidentate chelate (*e.g.* DOTA, 1,4,7,10-tetraazacyclododecane-1,4,7,10-tetraacetic acid) will be expected to yield a significant improvement in the aqueous stability, whilst also saturating the Ln^{III} coordination sphere as a 1 : 1 d–f complex, and these activities are also underway.

Conflicts of interest

There are no conflicts to declare.

Acknowledgements

Financial support by the Australian Research Council (DP170101895) is gratefully acknowledged.

Notes and references

1 M. D. Ward, *Coord. Chem. Rev.*, 2007, **251**, 1663–1677.

2 A. M. Nonat, C. Allain, S. Faulkner and T. Gunnlaugsson, *Inorg. Chem.*, 2010, **49**, 8449–8456.

3 W. S. Perry, S. J. A. Pope, C. Allain, B. J. Coe, A. M. Kenwright and S. Faulkner, *Dalton Trans.*, 2010, **39**, 10974–10983.

4 N. M. Tart, D. Sykes, I. Sazanovich, I. S. Tidmarsh and M. D. Ward, *Photochem. Photobiol. Sci.*, 2010, **9**, 886–889.

5 F.-F. Chen, Z.-Q. Bian, B. Lou, E. Ma, Z.-W. Liu, D.-B. Nie, Z.-Q. Chen, J. Bian, Z.-N. Chen and C.-H. Huang, *Dalton Trans.*, 2008, 5577–5583.

6 S. J. A. Pope, B. J. Coe, S. Faulkner and R. H. Laye, *Dalton Trans.*, 2005, 1482–1490.

7 S. I. Klink, H. Keizer and F. C. J. M. Van Veggel, *Angew. Chem., Int. Ed.*, 2000, **39**, 4319–4321.

8 K. Sénéchal-David, S. J. A. Pope, S. Quinn, S. Faulkner and T. Gunnlaugsson, *Inorg. Chem.*, 2006, **45**, 10040.

9 A. Beeby, I. M. Clarkson, R. S. Dickins, S. Faulkner, D. Parker, L. Royle, A. S. de Sousa, J. A. Gareth Williams and M. Woods, *J. Chem. Soc., Perkin Trans. 2*, 1999, 493–504.

10 T. Lazarides, D. Sykes, S. Faulkner, A. Barbieri and M. D. Ward, *Chemistry*, 2008, **14**, 9389–9399.

11 E. G. Moore, M. Benaglia, G. Bergamini and P. Ceroni, *Eur. J. Inorg. Chem.*, 2015, **2015**, 414–420.

12 E. A. Medlycott and G. S. Hanan, *Chem. Soc. Rev.*, 2005, **34**, 133–142.

13 J. M. Hamilton, M. J. Anhorn, K. A. Oscarson, J. H. Reibenspies and R. D. Hancock, *Inorg. Chem.*, 2011, **50**, 2764–2770.

14 A.-L. Gassner, C. Duhot, J.-C. G. Bünzli and A.-S. Chauvin, *Inorg. Chem.*, 2008, **47**, 7802–7812.

15 A. Aebischer, F. Gumy and J. C. Bunzli, *Phys. Chem. Chem. Phys.*, 2009, **11**, 1346–1353.

16 A. S. Chauvin, F. Gumy, D. Imbert and J. C. G. Bünzli, *Spectrosc. Lett.*, 2004, **37**, 517–532.

17 J. Andres and K. E. Borbas, *Inorg. Chem.*, 2015, **54**, 8174–8176.

18 H.-J. Park, S.-B. Ko, I. W. Wyman and S. Wang, *Inorg. Chem.*, 2014, **53**, 9751–9760.

19 J. Andres and A. S. Chauvin, *Phys. Chem. Chem. Phys.*, 2013, **15**, 15981–15994.

20 A. D'Aléo, A. Picot, P. L. Baldeck, C. Andraud and O. Maury, *Inorg. Chem.*, 2008, **47**, 10269.

21 R. Xiong, D. Mara, J. Liu, R. Van Deun and K. E. Borbas, *J. Am. Chem. Soc.*, 2018, **140**, 10975–10979.

22 J. Kim, D.-g. Kang, S. K. Kim and T. Joo, *Phys. Chem. Chem. Phys.*, 2020, **22**, 25811–25818.

23 G. Dehaen, S. V. Eliseeva, P. Verwilst, S. Laurent, L. Vander Elst, R. N. Muller, W. De Borggraeve, K. Binnemans and T. N. Parac-Vogt, *Inorg. Chem.*, 2012, **51**, 8775–8783.

24 S. Katagiri, R. Sakamoto, H. Maeda, Y. Nishimori, T. Kurita and H. Nishihara, *Chem. – Eur. J.*, 2013, **19**, 5088–5096.

25 C. J. Aspley and J. A. Gareth Williams, *New J. Chem.*, 2001, **25**, 1136–1147.

26 F. Barigelletti, L. Flamigni, V. Balzani, J.-P. Collin, J.-P. Sauvage, A. Sour, E. C. Constable and A. M. W. Cargill Thompson, *J. Am. Chem. Soc.*, 1994, **116**, 7692–7699.

27 C. Chakraborty, U. Rana, R. K. Pandey, S. Moriyama and M. Higuchi, *ACS Appl. Mater. Interfaces*, 2017, **9**, 13406–13414.

28 O. K. Rasheed, J. J. W. McDouall, C. A. Muryn, J. Raftery, I. J. Vitorica-Yrezabal and P. Quayle, *Dalton Trans.*, 2017, **46**, 5229–5239.

29 L. Alderighi, P. Gans, A. Ienco, D. Peters, A. Sabatini and A. Vacca, *Coord. Chem. Rev.*, 1999, **184**, 311–318.

30 H. S. Wang, B. Zhao, B. Zhai, W. Shi, P. Cheng, D. Z. Liao and S. P. Yan, *Cryst. Growth Des.*, 2007, **7**, 1851–1857.

31 E. Moore, *Dalton Trans.*, 2012, **41**, 5272–5279.

32 E. Jakubikova, W. Chen, D. M. Dattelbaum, F. N. Rein, R. C. Rocha, R. L. Martin and E. R. Batista, *Inorg. Chem.*, 2009, **48**, 10720–10725.

33 F. Barigelletti, L. Flamigni, G. Calogero, L. Hammarström, J.-P. Sauvage and J.-P. Collin, *Chem. Commun.*, 1998, 2333–2334.

34 M. Maestri, N. Armaroli, V. Balzani, E. C. Constable and A. M. C. Thompson, *Inorg. Chem.*, 1995, **34**, 2759–2767.

35 J. Andres and A.-S. Chauvin, *Inorg. Chem.*, 2011, **50**, 10082–10090.

36 J. Andres and A.-S. Chauvin, *Eur. J. Inorg. Chem.*, 2010, **2010**, 2700–2713.

37 E. G. Moore, J. Grilj, E. Vauthey and P. Ceroni, *Dalton Trans.*, 2013, **42**, 2075–2083.

38 A. T. Yeh, C. V. Shank and J. K. McCusker, *Science*, 2000, **289**, 935.

39 S. Faulkner, L. S. Natrajan, W. S. Perry and D. Sykes, *Dalton Trans.*, 2009, 3890–3979.